Journal of Applied Physics

RESEARCH ARTICLE | JUNE 08 2023

Topological wireless communication in the stopband of magnetoinductive lines

Joshua Feis ; Laszlo Solymar; Ekaterina Shamonina

Journal of Applied Physics 133, 223101 (2023)
https://doi.org/10.1063/5.0146831

Journal of Applied Physics ARTICLE scitation.org/journal/jap

Topological wireless communication in the stopband of magnetoinductive lines

Cite as: J. Appl. Phys. 133, 223101 (2023); doi: 10.1063/5.0146831
Submitted: 16 February 2023 · Accepted: 16 May 2023 ·
Published Online: 8 June 2023

Joshua Feis,[a] Laszlo Solymar, and Ekaterina Shamonina

AFFILIATIONS

Department of Engineering Science, University of Oxford, Oxford OX1 3PJ, United Kingdom

[a]**Author to whom correspondence should be addressed:** joshua.feis@eng.ox.ac.uk

ABSTRACT

Conventionally, in engineering, the stopband of periodic structures, where propagating signals are unable to penetrate them, was of little interest to engineers. However, with the advent of topological physics, this has changed, and the stopband has moved into the center of attention. Here, we study the behavior of magnetoinductive waves in the stopband of a diatomic line. Surprisingly, here, we find that for lines hosting topological edge states, the signal power at frequencies in the stopband can be higher than anywhere in the passband. Further, they may also exceed both the signal power and Shannon capacity of a conventional monoatomic line, making them of interest for application in wireless communication.

I. INTRODUCTION

Ever since their first appearance,[1,2] the properties of magnetoinductive waves have been widely investigated.[3,4] They are examples of simple periodic structures upon which signals can propagate. Dispersion equations have been derived exhibiting both forward and backward waves. Monoatomic and diatomic structures have been studied, showing that as a function of frequency, both structures possess passbands and stopbands. The main aim of this paper is a further study of these two bands. The concepts have been around for a long time. They were probably first identified by Lord Kelvin in his examinations of the properties of elastic waves.[5] When electrical filters were invented[6–8] at the beginning of the 20th century, the same phenomena were found and were given the same names. All electrical engineers became familiar with the concepts of passing and stopping signals as the frequency varied, whereas physicists encounter this during a thorough study of the more general case of periodic structures.[9] The terms passband and stopband are self-explanatory. Signals can pass in the passband but in the stopband they are unable to get through the line. The signal is stopped, or more precisely, using the proper technical term, one can say that the signal is an evanescent wave in the stopband. Hence, it is not surprising that there was no interest in studying the stopband. The situation changed, however, in the last decade, originating in the seemingly distant field of condensed matter theory. The stopband has moved into the center of attention.

It was found that, enforced and protected by fundamental mathematical rules, highly resonant and robust resonances called topological edge states may exist in the stopband.[10–13] Very surprisingly and contrary to all conventional wisdom, through the coupling of such edge states, one may wirelessly transmit power in the stopband efficiently and with higher robustness than in the passband, as prior work has shown.[14–16] As magnetoinductive waveguides used for wireless power transfer may also be used for wireless communication, a naturally arising proposition is to investigate the use of topological edge states for the purpose of communications. In this work, we show that the signal power transmitted by a suitably designed finite magnetoinductive line may also be very significant and, remarkably, higher in the stopband than anywhere in the passband.

To this end, we start by introducing our model capable of hosting topological edge states of magnetoinductive waves and then investigate and optimize the signal power it may be able to provide. We further show that such an approach provides multiple advantages over conventional magnetoinductive waveguides, leading to enhancements in both power output as well as an enhancement of the Shannon capacity of the link. Finally, we draw conclusions.

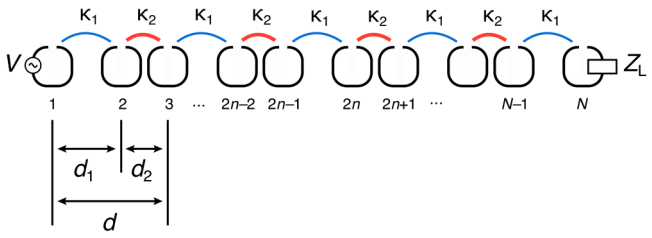

FIG. 1. Sketch of a diatomic magnetoinductive waveguide with coupling coefficients $\kappa_{1,2}$ line driven with a voltage V and loaded with an impedance Z_L.

II. MODEL

The model we consider in this work is a diatomic chain of meta-atoms with an even number of elements N, as illustrated in Fig. 1. Each element may be modeled as an *LCR* circuit with a self-impedance of

$$Z_0 = j\omega L + \frac{1}{j\omega C} + R = j\omega L\left(1 - \frac{\omega_0^2}{\omega^2} - j\frac{\omega_0}{\omega Q}\right), \tag{1}$$

where R denotes the resistance, L is the self-inductance, C is the capacitance, $\omega_0 = 1/\sqrt{LC}$ is the resonant frequency, and $Q = \omega_0 L/R$ is the quality factor of this circuit.[3] In this work, we assume nearest-neighbor coupling only, meaning that the coupling mechanism is mutual induction between pairs of adjacent resonators with mutual inductances $M_{1,2}$. Correspondingly, we define the coupling coefficients as

$$\kappa_{1,2} = 2\frac{M_{1,2}}{L}. \tag{2}$$

Let us briefly discuss and review the characteristics of such diatomic magnetoinductive lines.[3,17,18] We may assume that, for a line of infinite length, the currents follow the biperiodicity of the structure and can be written as

$$\begin{pmatrix} I_{2n} \\ I_{2n-1} \end{pmatrix} = \begin{pmatrix} Ae^{-jkn(d_1+d_2)} \\ Be^{-jkn(d_1+d_2)} \end{pmatrix}, \tag{3}$$

where A, B are complex current amplitudes and k is the wave number. Making use of Kirchhoff's equations for zero voltage

$$Z\mathbf{I} = 0, \tag{4}$$

with $\mathbf{I} = (I_1, \ldots, I_N)^T$ being the current vector and Z being the impedance matrix of the structure, where the impedance matrix elements for an unloaded chain are

$$Z_{nn} = Z_0, \tag{5}$$

as well as

$$Z_{nm} = j\omega M_{nm}, \qquad (n \neq m), \tag{6}$$

we find the dispersion equation as[3]

$$\cos kd = \frac{-Z_0^2 - \omega^2(M_1^2 + M_2^2)}{2\omega^2 M_1 M_2}. \tag{7}$$

In Fig. 2(a), we show the real and the imaginary part of $k = \beta - j\alpha$. We can see that as one might expect by analogy with, e.g., acoustic waves on diatomic chains, the dispersion splits into two passbands, where waves may propagate, separated by a stopband, where only evanescent waves exist.[17,19] At the center of the stopband $\omega = \omega_0$, these evanescent waves decay exponentially away from their excitation point as

$$e^{-\alpha d} = \left|\frac{\kappa_1}{\kappa_2}\right| \qquad (\kappa_2 > \kappa_1). \tag{8}$$

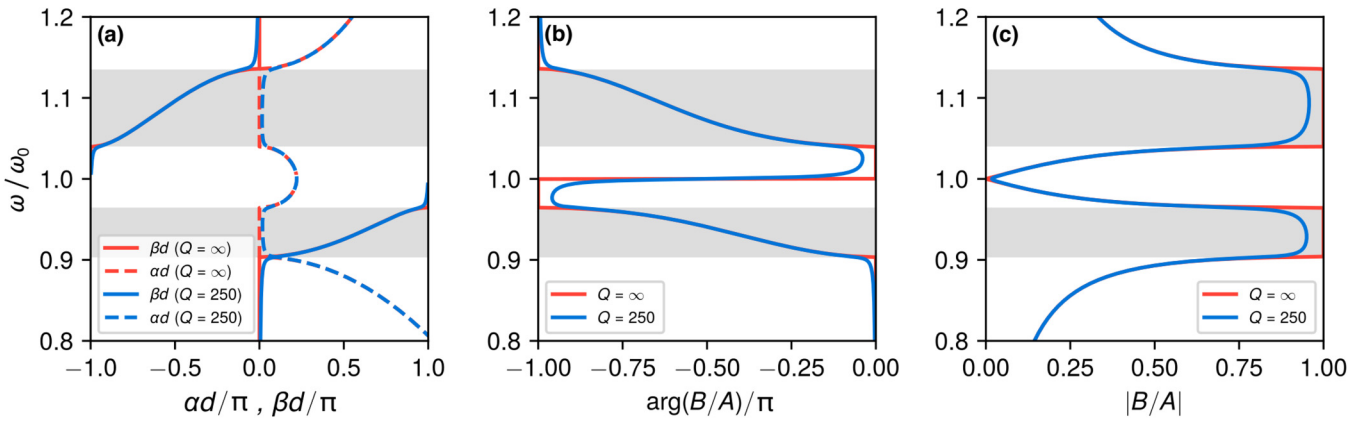

FIG. 2. Characteristics of an infinite-length diatomic magnetoinductive waveguide with $\kappa_1 = 0.15$ and $\kappa_2 = 0.3$. The shaded frequency ranges indicate the passbands. (a) Dispersion diagram for the real part of the wavenumber β and imaginary part α. (b) Phase ratio between neighboring sites $\arg(B/A)$. (c) Amplitude ratio between neighboring sites $|B/A|$.

The amplitudes of waves on each of the meta-atoms in the unit cell is found to be

$$\frac{B}{A} = -\frac{1}{2}\frac{\kappa_1 + \kappa_2 e^{-jkd}}{1 - \frac{\omega_0^2}{\omega^2} - j\frac{\omega_0}{\omega Q}} \tag{9}$$

In Figs. 2(b) and 2(c), we show the phase and the amplitude of this expression. The amplitude ratio of neighboring elements approaches unity in the passband with decreasing losses and vanishes in the stopband. Moreover, in further analogy to acoustic waves, for this choice of the signs of the coupling coefficients, in the lower passband the amplitudes of neighboring elements approach being in phase, whereas in the upper passband, they approach being in antiphase, corresponding to "acoustic" and "optical" bands, respectively. In the stopband, a phase jump occurs, with a phase difference of $-\pi/2$ right at the resonant frequency ω_0.[17]

So far, all these considerations have been for lines of infinite length. In a chain with a finite number of elements N, N resonances will occur at discrete points along the dispersion. For the chain of infinite length, all calculations so far were invariant with respect to interchange of the two coupling coefficients. This, however, ceases to be the case for a finite-length structure. Here, an additional quantity comes into play: the topological invariant of the chain.[20] As shown explicitly in prior works,[14,21] this model maps directly onto a Schrödinger-type problem of the form

$$\mathcal{H}\mathbf{I} = \frac{\omega_0^2}{\omega^2}[\mathbf{1}(1 + j\omega CR) - j\omega CZ]\mathbf{I}. \tag{10}$$

The matrix $\mathcal{H}$ is the equivalent of the Hamiltonian for this system, in the sense that it is a transformation of the impedance matrix into a matrix the eigenvalues of which are the eigenfrequencies of the system. Both Z and $\mathcal{H}$ are symmetric tridiagonal matrices, exactly like the matrix representation of the Hamiltonian of a tight-binding model with nearest-neighbor coupling. Correspondingly, this analog of a Hamiltonian $\mathcal{H}$ for our system turns out to directly map onto tight-binding models in 1D. Our two-band circuit model presented here is topologically equivalent to the Su–Schrieffer–Heeger (SSH) chain, a well-known model from solid-state physics that supports topological edge states.[10,20] Hence, we may also find its topological invariant, the winding number w to be

$$w = \frac{d}{2\pi}\int_{-\pi/d}^{\pi/d} \frac{\kappa_2 e^{jkd}}{\kappa_1 + \kappa_2 e^{jkd}}\,\mathrm{d}k = \begin{cases} 1 & \text{if } \kappa_2 > \kappa_1 \\ 0 & \text{if } \kappa_1 > \kappa_2 \end{cases}. \tag{11}$$

As for the SSH model, this invariant of the infinite chain then predicts whether for a chain of finite length any resonances, called topological edge states, will occur inside the stopband depending on whether the invariant vanishes or not.[22] Correspondingly, the theory of magnetoinductive waves contains topological states, in full analogy to, e.g., the theory of electron waves, where these were initially conceived. Taking full advantage of this parallelism and the superior experimental and theoretical accessibility of such microwave systems, magnetoinductive chains like this have previously been used to study edge states, though only very recently with a focus on applications rather than proofs-of-principle.[23–25]

Finally, in order to actually excite our structure and deliver a signal, the voltage $\mathbf{V} = (1, \ldots, 0)^{\mathrm{T}}$ V is applied and the last element is equipped with an additional, carefully chosen load impedance Z_{L}. Hence, the calculations in this work are taking into account that this is an open system with power input and output. From Kirchhoff's law, we can then find all currents in the system as

$$\mathbf{I} = Z^{-1}\mathbf{V}. \tag{12}$$

III. RESULTS AND DISCUSSION

With these preliminaries in place, we can begin our investigation. As a key figure of merit for a wireless link, in our system, we may calculate the signal power P seen by the receiving load impedance at the end of the chain as

$$P = \frac{1}{2}\mathrm{Re}(Z_{\mathrm{L}})|I_N|^2, \tag{13}$$

where I_N denotes the current in the last element. This quantity is the target of our optimization. For the sake of making our calculations definite, we choose realistic fixed values for the resonant frequency, $\omega_0 = 10\,\mathrm{MHz}$, the quality factor $Q = 250$, and inductance $L = 7\,\mu\mathrm{H}$. The remaining free parameters, the coupling coefficients as well as the load impedance, are now to be optimized. To do this properly, we have to first establish a benchmarking procedure for this type of near-field communication. Whether a platform is suitable for transmitting signals is determined by two interlinked factors, namely its transmission distance and the signal strength it manages to transmit over this distance. Clearly, they are related, as typically signal power decreases with increasing transmission distance, to which our platform is no exception. This means that when comparing different realizations of magnetoinductive waveguides, we ought to compare chains of equal length. The length of the chain is (almost, assuming small meta-atoms compared to their separation, which is true in our case) exclusively determined by the coupling (or *vice versa*), which approximately scales as

$$\kappa \propto \frac{1}{d^3}, \tag{14}$$

where d is the spacing between two resonant elements. This is valid given the elements are not packed too tightly, which for the purpose of wireless signaling they, of course, should not be. Correspondingly, using Eq. (14), we find that to ensure equal chain length and thus transmission distance

$$\sum_i^N \kappa_i^{-1/3} = \sum_i^N \tilde{\kappa}_i^{-1/3}, \tag{15}$$

where κ_i and $\tilde{\kappa}_i$ are the coupling coefficients of two different chains, should hold.

In Fig. 3, the optimized signal power for a chain of length $N = 8$ is shown. For every frequency, the optimal, i.e., matched, the load impedance is determined numerically. As explained above,

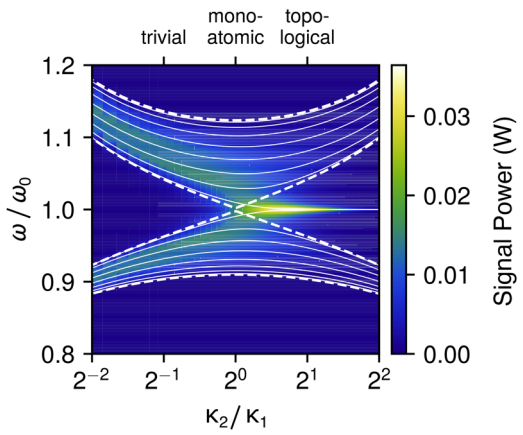

FIG. 3. Signal power optimization of coupling ratio κ_2/κ_1 for constant transmission distance. The optimal load impedance is determined independently at every frequency point. The dashed lines show the edges of the passbands and the solid lines correspond to the eigenfrequencies of the system.

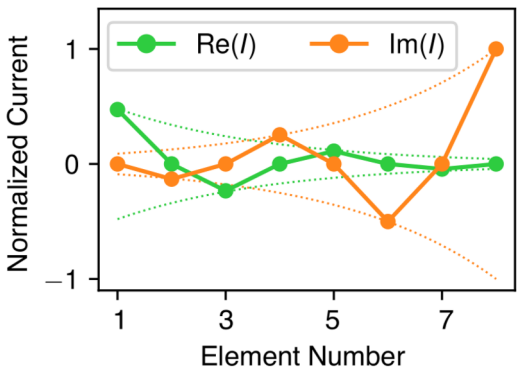

FIG. 4. Normalized real and imaginary part of current I at $\omega = \omega_0$ for optimal signal transmission via coupled topological edge states. The dotted lines show fitted exponential functions enveloping the real and imaginary parts of the current, showing the exponential nature of the amplitude decay away from the edges of the chain.

the transmission distance is fixed, meaning in this case we required a constant $\kappa_1^{-1/3} + \kappa_2^{-1/3} \approx 3.38$, ensuring that chains with different coupling coefficients are comparable. We can clearly see the presence of the two passbands separated by the bandgap that opens and widens with increased deviation from the case of equal couplings, meaning a monoatomic chain. Crucially, for $\kappa_2/\kappa_1 \approx 2$, i.e., in the topologically nontrivial regime, we see a pronounced global maximum of the signal power in the center of the stopband. This is indeed due to topological edge states present at the center of the stopband coupling via their evanescent tails, as we illustrate in Fig. 4. There, we show the normalized current for each of the elements. It can clearly be seen how the edge state excited on the left edge (located on the sublattice of even-numbered elements) feeds the edge state on the right (located on the sublattice of odd-numbered elements) with its maximum located right on the loaded element. This is happening via evanescent magnetoinductive waves decaying from either end of the structure into the bulk, as indicated by the dotted lines as given by Eq. (8). Fundamentally, this behavior is quite reminiscent of the earlier example of surface plasmon polaritons excited at the two opposing surfaces of a thin silver slab.[26,27] In Fig. 5, we plot a cut through the optimization plot at the coupling ratio of the global maximum ($\kappa_2/\kappa_1 = 2$) as well as for its inverse ($\kappa_2/\kappa_1 = 1/2$) and equal couplings ($\kappa_2/\kappa_1 = 1$). We can clearly see that the maximum power is significantly larger for the topological chain than it is for both the monoatomic chain with equal couplings as well as the topologically trivial chain with swapped coupling coefficients. We note that this persists when the fixed transmission distance is not required, meaning even a quite significant increase in coupling and hence reduction in chain length do not lead to a maximum signal power exceeding that of a shorter topological chain. We emphasize here that this is not the point of maximum efficiency as the maximum power transfer theorem states that it is either power or efficiency that can be maximized but never both at the same time. Previous work has also shown that in terms of efficiency, topological chains like ours here while comparable usually do not outperform their monoatomic counterparts. The enhancement of the signal power through using the topological chain instead of, for example, the monoatomic chain also stays robust against coupling disorder. In Fig. 6, we show the average ratio of signal power delivered by the topological chain over the signal power delivered by the monoatomic chain when

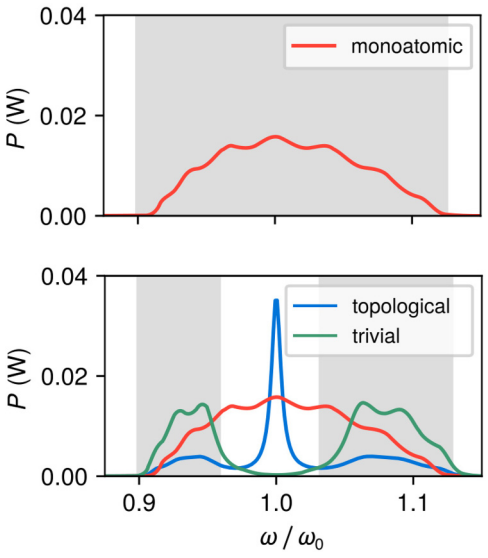

FIG. 5. Optimized signal power for coupling ratios of $\kappa_2/\kappa_1 = 2$ as well as the monoatomic case with $\kappa_2/\kappa_1 = 1$. The peak signal power for the topological chain significantly exceeds the power for the monoatomic chain and the trivial chain (i.e., the topological chain with swapped couplings). The shaded frequency ranges indicate the passbands.

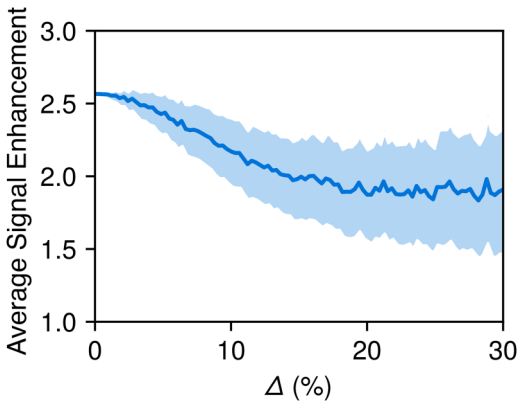

FIG. 6. Average signal power enhancement factor achieved by the topological chain compared to the monoatomic chain as a function disorder. The area shaded in blue indicates the standard deviation of the enhancement factor. Due to the protection of the topological edge state against this type of disorder, the enhancement is robust against it.

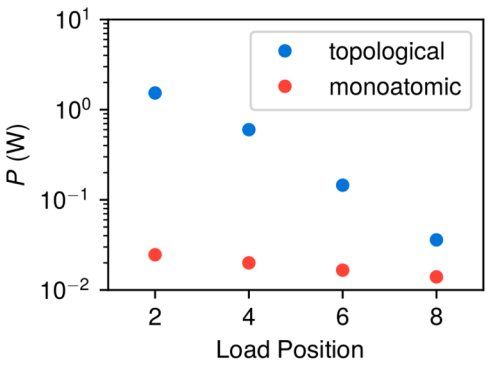

FIG. 7. Variation of the signal power for the topological chain as well as the monoatomic chain with varying position of the load on one sublattice from unit cell adjacent to excitation to end of the chain. For each position of the load, the topological chain supplies a higher signal power than the monoatomic chain.

randomly varying the distance between all elements n and m according to

$$d_{nm} = (1 + \delta_{nm}), \tag{16}$$

with the perturbation δ_{nm} randomly distributed in the interval $(-\Delta, \Delta)$. Clearly, despite the disorder increasing to significant values, the topological chain consistently outperforms its conventional monoatomic counterpart. This is due to the edge state being robust against this type of coupling disorder, which does not break the chiral symmetry of the system.

We also note and would like to show in the following that a very useful property of these types of magnetoinductive waveguides is preserved for the topological chains, namely, random accessibility. With the term random accessibility, we specifically mean that the power may be taken out of every unit cell by moving the load, implying a significant advantage in flexibility and reconfigurability compared to, for instance, a wire-based transmission setup. The load for magnetoinductive waveguides is often a movable loaded element, meaning that in most cases, this flexibility should prove useful. In Fig. 7, one can see that even as the load impedance is moved along the chain (albeit here with the restriction of accessing the same element in each unit cell every time), the power output of the topological chain is consistently higher than that of the conventional monoatomic chain. As a matter of fact, the closer the load is to the excitation, the more strongly enhanced the output power is, which can be understood in terms of the evanescent coupling to the edge state, which vanishes more rapidly as the number of elements and thus the distance between load and excitation is increased. We mention here that this eventually also places a limit on the applicability of our proposal: for a sufficiently long chain, where the precise length is determined by the losses, the signal transmission through the topological chain becomes weaker than through the conventional chain as the evanescent coupling with the edge state becomes exceedingly small. Potential strategies to mitigate this are subject of the ongoing work.

With a view of applications, this significant and robust enhancement of power output may prove useful in schemes where this raw power is most important, such as, for example, radio-frequency identification (RFID), where exceeding a threshold power level is essential to activate a passive transponder and ultimately determines the distance over which it may be used.[28] In a somewhat different avenue of applications, we point out that this may also be of use for localized microwave heating, since as we show in Fig. 4, the increase in output power is due to the localized maximum in current at the end of the chain, which, in turn, directly implies maximum heat dissipation in that element while the other elements dissipate considerably less heat, something that is desirable for instance for some biomedical applications.[29,30] Primarily though, and hence subject to further discussion in the following, we envision that this enhanced signal power will find its application in communication, where stronger signals are amongst the foremost optimization targets for the construction of any communication link.

For the purpose of communications schemes, we know that an additional variable plays a role in determining the performance of a given link: the bandwidth. From the optimal power curve in Fig. 5, it may be tempting to argue that the wider-band nature of conventional links could offset the increased signal power of the topological link. In a real setup that would not be the case, as the receiver load would be fixed (and hence, only perfectly matched for that one specific frequency) leading to a far more rapid drop-off in signal strength when going off the operating frequency. We show this in Fig. 8, where we take the same couplings as in Fig. 5 but assume a fixed resistive load, in this case $Z_L = (10 + 0.5\mathrm{j})\,\Omega$ for the topological and $Z_L = (150 - 0.5\mathrm{j})\,\Omega$ for the monoatomic chain, is optimal for power output at ω_0. As can be seen clearly, the power while of course identical at the center frequency drops off far more rapidly with such a fixed load, leading to a much narrower bandwidth than if the load impedance was perfectly optimized for each frequency. Quantitatively, the law describing the capacity c of a channel that derives from signal power and bandwidth is the

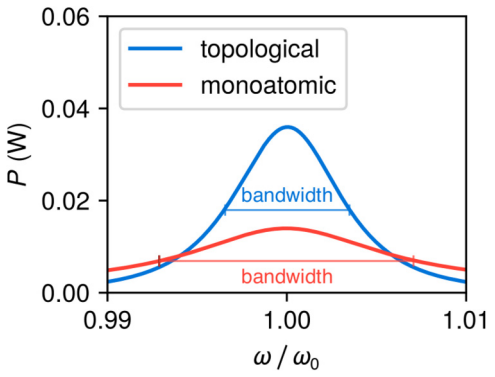

FIG. 8. Signal power for the case of non-dispersive resistive load optimized for the operation at ω_0. In this case, the signal power drops off significantly faster leading to a smaller bandwidth, the definition of which is illustrated in this figure.

Shannon–Hartley theorem[31]

$$c = \int_{\omega_0 - B/2}^{\omega_0 + B/2} \log_2 \left[1 + \frac{P(\omega)}{N_0} \right] \mathrm{d}\omega, \tag{17}$$

where N_0 is the spectral density for the noise power, which here we assume to be independent of frequency and B is the bandwidth, i.e., full width at half maximum of the power around the operating frequency ω_0 as illustrated in Fig. 8. This additional variable of the bandwidth now means that the answer of which link performs better in terms of the Shannon capacity is, despite the typically higher maximum signal power of the topological chain, not directly obvious anymore. As can be seen in Fig. 9, the monoatomic chain generally gives a wider bandwidth, though this becomes particularly pronounced at low quality factors, where it rapidly increases as all spectral features broaden due to losses. Such an increase can also be seen for the topological chain, though there it is less pronounced. On the other hand though, looking at Fig. 10, we can see that, with an increasing quality factor, the signal power of the topological chain significantly outscales its conventional counterpart. The insets show the current profile associated with each chain for a low quality factor as well as a high quality factor. While, for the monoatomic chain, the current profile remains flat and thus essentially qualitatively independent from losses, we can see that for the topological chain, there is a significant increase in current on the receiving element hosting the topological edge state, correspondingly also leading to an increase in signal power. We note here—in a glance beyond communications—that this type of current profile could also be attractive for applications where localized power delivery is desirable, such as wireless but targeted heating. For the Shannon capacity, these different scaling behaviors of decreasing bandwidth but increasing power for the two chains mean that there is no immediate answer as to which chain performs better. To answer this, in Fig. 11, we show the enhancement of the Shannon capacity for a topological chain over a conventional monoatomic one as a function of both quality factor as well as noise power N_0. First, we can clearly see that below a quality factor of around 180, the conventional chain always performs better. This is to be expected as the power advantage of the topological chain is not significant enough there to make up the bandwidth disadvantage. Second, for lower noise powers, the conventional chain again performs better. This is due to the scaling behavior of the Shannon capacity, where with decreased noise power the capacity is limited

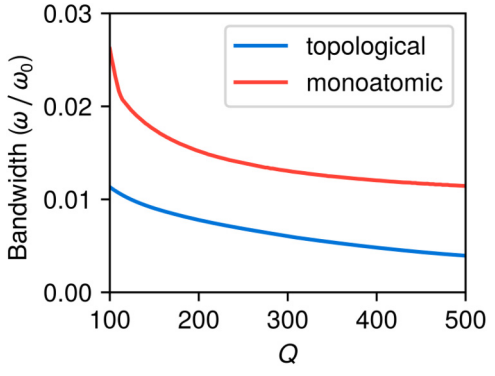

FIG. 9. Scaling of the bandwidth with losses. For a low quality factor meaning high losses, the bandwidth of the monoatomic chain rapidly increases while for lower losses, it drops off at a rate similar to the topological chain, though the monoatomic chain bandwidth consistently exceeds the bandwidth of the topological chain.

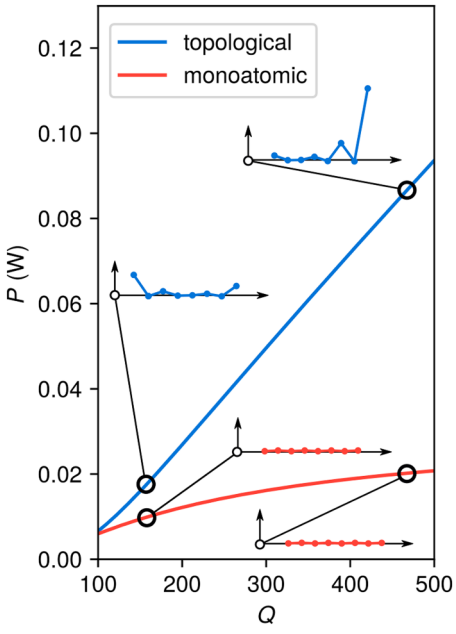

FIG. 10. Scaling of optimum output power with losses. When varying the quality factor Q, it can clearly be seen that, as Q increases the topological chain (blue) exponentially outscales the conventional one. The inset shows the behavior of the currents as the quality factor increases.

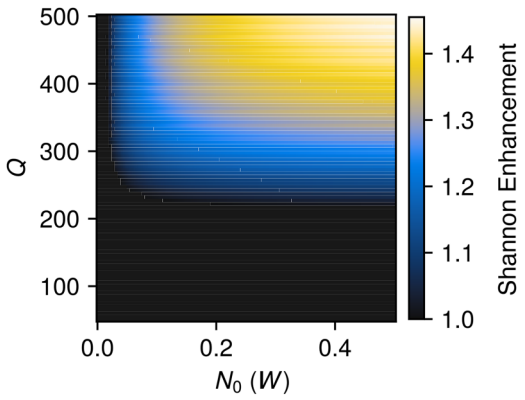

FIG. 11. Enhancement of the Shannon capacity for the topological chain compared to the monoatomic chain for varying quality factor Q and different noise powers. The color scale is limited with a lower limit of 1, where signal transmission using the topological chain is just as good or worse than with the conventional scale.

more by the bandwidth than the power, favoring the conventional system. For a sufficiently high noise power and above a certain value of the quality factor though, the topological chain is indeed outperforming the conventional chain in terms of the Shannon capacity. We can clearly see that the higher either noise or quality factor are in this regime, the more pronounced this advantage becomes, ranging in our limits up to almost 50% enhancement.

Hence, this clearly shows that, in a high noise regime and given reasonably but realistically low losses, magnetoinductive wave communication links may indeed be improved by using the topological chain instead of the conventional monoatomic one.

IV. CONCLUSIONS

In conclusion, we have proposed and investigated the advantages of the use of topological edge states in diatomic magnetoinductive waveguides for use in wireless communications. We have shown that an evanescently excited topological edge state may provide significant enhancements in signal power compared to conventional, monoatomic setups utilizing propagating waves. The random accessibility of magnetoinductive waveguides stays intact also for such topological chains. This could prove useful to a range of applications such as communications but also beyond that in applications where such peaks in power are desirable like RFID,[28] heating[29,30] or sensing.[32] We have further shown that despite the reduction in bandwidth due to the resonant nature of the topological edge state, the signal power enhancement is large enough that in a scenario with sufficiently low losses and high noise, it leads to a notable enhancement of the Shannon capacity of the magnetoinductive communications link.

SUPPLEMENTARY MATERIAL

See the supplementary material for a detailed derivation of Eqs. (7)–(9).

ACKNOWLEDGMENTS

We are grateful to colleagues from the OxiMeta network and the Oxford Communications Engineering group for fruitful discussions, in particular, Professor Christopher J. Stevens. We acknowledge financial support by the Engineering and Physical Sciences Research Council (EPSRC) (Grant No. EP/N010493/1 SYMETA). J.F. acknowledges support by the University of Oxford through a Scatcherd European Scholarship and by the Engineering and Physical Sciences Research Council (EPSRC) through a Doctoral Training Account.

AUTHOR DECLARATIONS

Conflict of Interest

The authors have no conflicts to disclose.

Author Contributions

Joshua Feis: Conceptualization (equal); Formal analysis (equal); Investigation (equal); Methodology (equal); Software (equal); Validation (equal); Writing – original draft (equal); Writing – review & editing (equal). **Laszlo Solymar:** Conceptualization (equal); Formal analysis (equal); Investigation (equal); Validation (equal); Writing – review & editing (equal). **Ekaterina Shamonina:** Conceptualization (equal); Formal analysis (equal); Funding acquisition (equal); Investigation (equal); Methodology (equal); Supervision (equal); Writing – review & editing (equal).

DATA AVAILABILITY

The data that support the findings of this study are available from the corresponding author upon reasonable request.

REFERENCES

[1]E. Shamonina, V. Kalinin, K. Ringhofer, and L. Solymar, "Magnetoinductive waves in one, two, and three dimensions," J. Appl. Phys. **92**, 6252–6261 (2002).
[2]M. Wiltshire, E. Shamonina, I. Young, and L. Solymar, "Dispersion characteristics of magneto-inductive waves: Comparison between theory and experiment," Electron. Lett. **39**, 1 (2003).
[3]L. Solymar and E. Shamonina, *Waves in Metamaterials* (Oxford University Press, Oxford, 2009).
[4]R. Marqués, F. Martin, and M. Sorolla, *Metamaterials with Negative Parameters: Theory, Design, and Microwave Applications* (John Wiley & Sons, 2011).
[5]W. Thomson and B. Kelvin, *Baltimore Lectures on Molecular Dynamics and the Wave Theory of Light* (Cambridge University Press, 1904).
[6]K. W. Wagner, "Die Theorie des Kettenleiters nebst Anwendungen. (Wirkung der verteilten Kapazität in Widerstandssätzen)," Arch. Electrotech. **3**, 315–332 (1915).
[7]G. A. Campbell, "Physical theory of the electric wave-filter," Bell Syst. Tech. J. **1**, 1–32 (1922).
[8]W. Cauer, "Die Verwirklichung von Wechselstromwiderständen vorgeschriebener Frequenzabhängigkeit," Arch. Electrotech. **17**, 355–388 (1926).
[9]L. Brillouin, *Wave Propagation and Group Velocity* (Academic Press, New York, 1960).
[10]W. Su, J. Schrieffer, and A. J. Heeger, "Solitons in polyacetylene," Phys. Rev. Lett. **42**, 1698 (1979).

[11]D. J. Thouless, M. Kohmoto, M. P. Nightingale, and M. den Nijs, "Quantized Hall conductance in a two-dimensional periodic potential," Phys. Rev. Lett. **49**, 405 (1982).
[12]M. V. Berry, "Quantal phase factors accompanying adiabatic changes," Proc. R. Soc., Lond., Ser. A **392**, 45–57 (1984).
[13]Q. Niu, D. J. Thouless, and Y.-S. Wu, "Quantized Hall conductance as a topological invariant," Phys. Rev. B **31**, 3372 (1985).
[14]J. Feis, C. Stevens, and E. Shamonina, "Wireless power transfer through asymmetric topological edge states in diatomic chains of coupled meta-atoms," Appl. Phys. Lett. **117**, 134106 (2020).
[15]J. Song, F. Yang, Z. Guo, X. Wu, K. Zhu, J. Jiang, Y. Sun, Y. Li, H. Jiang, and H. Chen, "Wireless power transfer via topological modes in dimer chains," Phys. Rev. Appl. **15**, 014009 (2021).
[16]L. Zhang, Y. Yang, Z. Jiang, Q. Chen, Q. Yan, Z. Wu, B. Zhang, J. Huangfu, and H. Chen, "Demonstration of topological wireless power transfer," Sci. Bull. **66**, 974–980 (2021).
[17]O. Sydoruk, O. Zhuromskyy, E. Shamonina, and L. Solymar, "Phonon-like dispersion curves of magnetoinductive waves," Appl. Phys. Lett. **87**, 072501 (2005).
[18]O. Sydoruk, A. Radkovskaya, O. Zhuromskyy, E. Shamonina, M. Shamonin, C. Stevens, G. Faulkner, D. Edwards, and L. Solymar, "Tailoring the near-field guiding properties of magnetic metamaterials with two resonant elements per unit cell," Phys. Rev. B **73**, 224406 (2006).
[19]A. Radkovskaya, O. Sydoruk, M. Shamonin, E. Shamonina, C. Stevens, G. Faulkner, D. Edwards, and L. Solymar, "Experimental study of a bi-periodic magnetoinductive waveguide: Comparison with theory," IET Microw. Antennas Propag. **1**, 80–83 (2007).
[20]M. Z. Hasan and C. L. Kane, "Colloquium: Topological insulators," Rev. Mod. Phys. **82**, 3045 (2010).
[21]Y. Nakata, T. Okada, T. Nakanishi, and M. Kitano, "Circuit model for hybridization modes in metamaterials and its analogy to the quantum tight-binding model," Phys. Status Solidi B **249**, 2293–2302 (2012).
[22]J. K. Asbóth, L. Oroszlány, and A. Pályi, "A short course on topological insulators," Lect. Notes Phys. **919**, 166 (2016).
[23]J. Jiang, Z. Guo, Y. Ding, Y. Sun, Y. Li, H. Jiang, and H. Chen, "Experimental demonstration of the robust edge states in a split-ring-resonator chain," Opt. Express **26**, 12891–12902 (2018).
[24]Z. Guo, H. Jiang, Y. Sun, Y. Li, and H. Chen, "Asymmetric topological edge states in a quasiperiodic harper chain composed of split-ring resonators," Opt. Lett. **43**, 5142–5145 (2018).
[25]J. Jiang, J. Ren, Z. Guo, W. Zhu, Y. Long, H. Jiang, and H. Chen, "Seeing topological winding number and band inversion in photonic dimer chain of split-ring resonators," Phys. Rev. B **101**, 165427 (2020).
[26]E. Shamonina, V. Kalinin, K. Ringhofer, and L. Solymar, "Imaging, compression and Poynting vector streamlines for negative permittivity materials," Electron. Lett. **37**, 1 (2001).
[27]N. Fang, Z. Liu, T.-J. Yen, and X. Zhang, "Regenerating evanescent waves from a silver superlens," Opt. Express **11**, 682–687 (2003).
[28]Z. N. Chen, *Antennas for Portable Devices* (John Wiley & Sons, 2008).
[29]Z. Wu, B. Deng, J. Liu, and B. Zeng, "Highly efficient microwave heating for target area based on metamaterial," Microw. Opt. Technol. Lett. **59**, 758–761 (2017).
[30]M. J. Freire and R. Marqués, "Planar magnetoinductive lens for three-dimensional subwavelength imaging," Appl. Phys. Lett. **86**, 182505 (2005).
[31]A. Goldsmith, *Wireless Communications*, 1st ed. (Cambridge University Press, 2005).
[32]Z. Guo, T. Zhang, J. Song, H. Jiang, and H. Chen, "Sensitivity of topological edge states in a non-hermitian dimer chain," Photonics Res. **9**, 574–582 (2021).